

High-performance soft x-ray spectromicroscopy beamline at SSRF

Chaofan Xue, Yong Wang, Zhi Guo, Yanqing Wu, Xiangjun Zhen et al.

Citation: *Rev. Sci. Instrum.* **81**, 103502 (2010); doi: 10.1063/1.3491837

View online: <http://dx.doi.org/10.1063/1.3491837>

View Table of Contents: <http://rsi.aip.org/resource/1/RSINAK/v81/i10>

Published by the [American Institute of Physics](#).

Related Articles

Elemental and magnetic sensitive imaging using x-ray excited luminescence microscopy
Rev. Sci. Instrum. **83**, 073701 (2012)

A cryogenic circulating advective multi-pass absorption cell
Rev. Sci. Instrum. **83**, 035104 (2012)

A simple external resistance heating diamond anvil cell and its application for synchrotron radiation x-ray diffraction
Rev. Sci. Instrum. **81**, 053903 (2010)

SAMRAI: A novel variably polarized angle-resolved photoemission beamline in the VUV region at UVSOR-II
Rev. Sci. Instrum. **81**, 053104 (2010)

Calculations of synchrotron radiation emission in the transverse coherent limit
Rev. Sci. Instrum. **80**, 106103 (2009)

Additional information on *Rev. Sci. Instrum.*

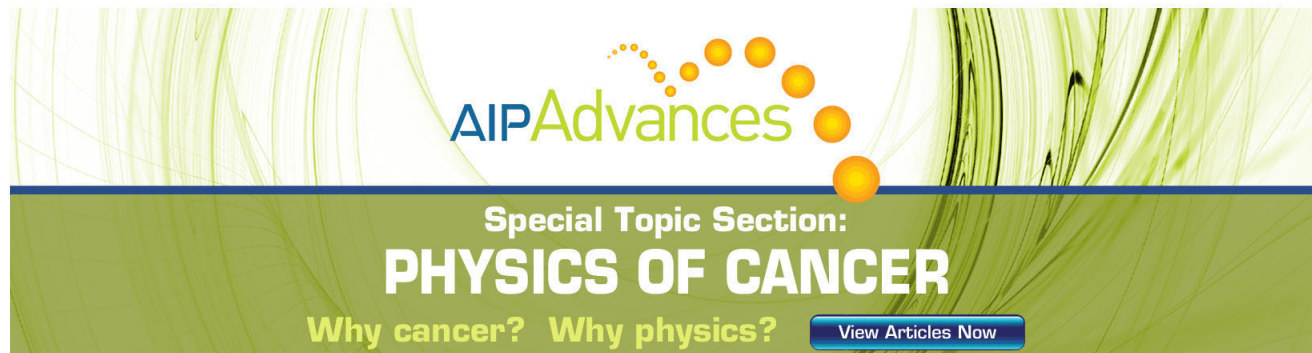
Journal Homepage: <http://rsi.aip.org>

Journal Information: http://rsi.aip.org/about/about_the_journal

Top downloads: http://rsi.aip.org/features/most_downloaded

Information for Authors: <http://rsi.aip.org/authors>

ADVERTISEMENT



AIPAdvances

Special Topic Section:
PHYSICS OF CANCER

Why cancer? Why physics? [View Articles Now](#)

High-performance soft x-ray spectromicroscopy beamline at SSRF

Chaofan Xue,¹ Yong Wang,¹ Zhi Guo,¹ Yanqing Wu,¹ Xiangjun Zhen,¹ Min Chen,¹ Jiahua Chen,¹ Song Xue,¹ Zhongqi Peng,² Qipeng Lu,² and Renzhong Tai^{1,a)}

¹Shanghai Institute of Applied Physics, Chinese Academy of Sciences,
Shanghai Synchrotron Radiation Facility, Shanghai 201800, China

²Changchun Institute of Optics, Fine Mechanics and Physics,
Chinese Academy of Sciences, Changchun 130033, China

(Received 23 April 2010; accepted 27 August 2010; published online 20 October 2010)

The Shanghai Synchrotron Radiation Facility (SSRF) is the first third-generation synchrotron facility in China and operated at an electron energy of 3.5 GeV. One of the seven beamlines in the first construction phase is devoted to soft x-ray spectromicroscopy and is equipped with an elliptically polarized undulator light source, a plane grating monochromator, and a scanning transmission x-ray microscope end station. Initial results reveal the high performance of this beamline, with an energy resolving power estimated to be over 10 000 at the argon L-edge and a spatial resolution better than 30 nm. © 2010 American Institute of Physics.

[doi:[10.1063/1.3491837](https://doi.org/10.1063/1.3491837)]

I. INTRODUCTION

Many scientific research areas require chemical analysis with submicron spatial resolution. However, well-established chemically sensitive methods such as infrared spectroscopy or nuclear magnetic resonance spectroscopy lack high spatial resolution. By contrast, electron microscopy has excellent spatial resolution but has minimal elemental or chemical sensitivity. Furthermore, its use is often prohibited for radiation-sensitive samples due to the strong radiation damages induced by the electrons. X-ray spectromicroscopy is a technique using high brilliant tunable synchrotron radiation and allows for both spatial resolution and chemical sensitivity. This technique exhibits a sub-100 nm resolving ability in space, as determined by the zone plate and a chemical distinguishing ability determined by the beamline monochromator via near edge x-ray absorption fine structure (NEXAFS) spectroscopy. So far, several such scanning transmission x-ray microscope (STXM) instruments have been built in different synchrotron radiation facilities (e.g., ALS, CLS, BESSY, SLS) and have eventually become important tools for scientific research.^{1–7}

The Shanghai Synchrotron Radiation Facility (SSRF) is the first third-generation synchrotron in China and operates at an electron energy of 3.5 GeV and with a beam current of 200 mA. The soft X-ray Spectromicroscopy Beamline (BL08U) is the only soft x-ray beamline among the seven beamlines in the first construction phase. It consists of an APPLE-II type, elliptically polarized undulator (EPU), two mirrors [a cylindrical mirror before and a toroidal mirror after the plane grating monochromator (PGM)], an entrance-slitless PGM [two gratings: 800 l/mm Pt coated (optimized for 250–750 eV); 1200 l/mm Au coated (optimized for 275–2000 eV)], and an experimental station equipped with a

STXM. To satisfy the requirements for most users, the photon energy was chosen to range from 250 to 2000 eV, thereby covering the K-edge of C, N, O, F, Na, Mg, Al, and Si, and the L edges of P, S, Cl, K, Ca, Fe, Cu, and Zn, which are important in biological science, environmental science, and polymer and material science.^{8–11} In addition, the light source is an elliptical polarized undulator, which allows for more opportunities to study polarization-dependent materials. The end station was designed to have a small beam spot down to 50 nm and be able to measure the transmitted NEXAFS, the 2D and the 3D scanning transmission image, and the total electron yield.

II. BEAMLINE LAYOUT

The layout of the beamline is shown in Fig. 1. A 4.2 m long APPLE-II type elliptically polarized undulator with 100 mm periods is used to produce high brilliant soft x-ray photons with variable polarization. By shifting these two diagonal rows longitudinally with respect to the fixed rows, the polarization state of the emitted photons can be tuned to be circular, elliptical, or linear (horizontal or vertical). The photon energy is chosen by changing the gap distance between the upper and lower pairs of magnetic rows. The first and third harmonics basically cover the needed photon energy range. Figure 2 shows a representative emitted spectrum with the EPU gap set at 55.49 mm, corresponding to an energy of 250 eV for the first harmonic. The 7th harmonic was obtained in this experiment, but the 9th or 11th harmonic can be reached in practice. A theoretical curve is fitted to the data, showing that the lower harmonic closely matches the theoretical values. By contrast, the higher-order harmonic exhibits some discrepancies because of the phase error, which describes the phase distribution of emissions from each undulator pole.

A four-jaw aperture (slit 1) located at 20 m from the source point was employed to define the acceptance angle of

^{a)} Author to whom correspondence should be addressed. Electronic mail: tairenzhong@sinap.ac.cn.

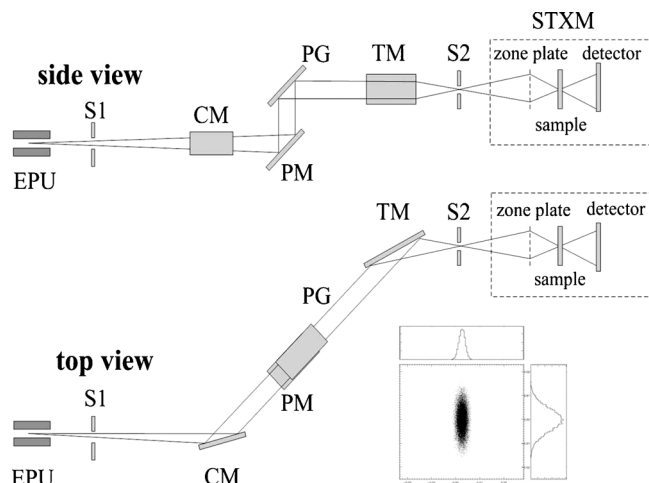


FIG. 1. Schematic layout of the BL08U beamline. The SHADOW ray-tracing result shows the beam spot at the exit slit.

the beamline, that is ± 0.04 mrad in the horizontal and vertical directions. The slit also functions to absorb most of the heat load and to protect the downstream optical elements. The key instrument of the beamline is the plane grating monochromator,^{12–14} before which a cylindrical mirror was used to produce a parallel beam in vertical and deflect the incoming beam horizontally by 3.44° . This mirror was Au coated and side-water cooled, and also played a role in cutting the higher harmonic radiation (>2000 eV). The PGM (SX700 type) is operated in collimated mode. This device is ideal for downstream optics and makes photon tuning easier just by changing its included angle while keeping its incoming and outgoing axes the same. To guarantee mechanical accuracy during grating switching, the two gratings were designed to be fabricated on one substrate. An internally water-cooled scheme was adopted for the premirror to protect the surface from the high heat load during photon tuning (rotation). The plane mirror substrate size is 80 mm wide, 450 mm long, and 75 mm thick. It is composed of two pieces that are permanently bound together. The water channels (32 channels combined into four groups of eight channels each with a channel width and height of 1 and 5 mm, respectively) are in the faceplate. The hot wall thickness is about 1.5 mm.

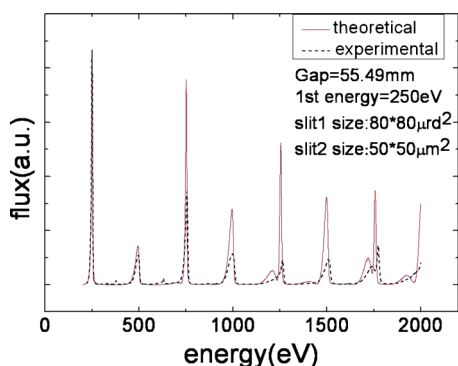


FIG. 2. (Color online) An EPU spectrum curve measured with grating 2 (1200 l/mm) using a photodiode after the exit slit. The four-jaw aperture (slit 1) and exit slits (slit 2) were $1600\ \mu\text{m} \times 1600\ \mu\text{m}$ and $50\ \mu\text{m} \times 50\ \mu\text{m}$, respectively. The EPU gap was set at 55.49 mm, which corresponds to the first harmonic energy of 250 eV.

The nominal water flow rate is up to $1.2 \times 10^{-4}\ \text{m}^3/\text{s}$ (1.9 U.S. gallons/min), which leads to a pressure drop of approximately 193 kPa (28 psi) inside the mirror. The C_{ff} value of this PGM was designed to be adjustable from 1.8 to 2.5, which makes it possible to select the desired mode, such as higher flux, higher harmonic suppression, and higher energy resolving power. The beam offset and mechanical precision were designed to be 30 mm and better than 0.42 arc sec, respectively. The last optical element was a toroidal mirror, which refocuses the beam simultaneously in the horizontal and vertical directions at the exit slit (slit 2). The exit slit also acts as a secondary light source for the zone plate at the end station, and its width determines the spatial resolution of the microscope. All the measurements were carried out at a condition of 50 by $50\ \mu\text{m}$ exit slit width, if not particularly emphasized. The SHADOW ray-tracing result in Fig. 1 shows the influence of the aberrations from optical elements. Calculations were done using the -1 order diffraction of the 1200 l/mm grating at 250 eV.

A commercial STXM (produced by Xradia) was permanently installed at the end station, consisting of a focusing optics module, sample module, and detector module. For STXM, the beam size at the zone plate was chosen to be two times larger than the zone plate width ($200\ \mu\text{m}$) to maintain phase matching. The STXM chamber is isolated from the upstream ultrahigh vacuum with a 100 nm thick Si_3N_4 window. The focusing optics module consists of a XYZ stage stack and holds the zone plate used to focus the x-ray beam. A smaller XYZ stage stack supporting the order-sorting aperture (OSA) is located on top of the zone plate stage stack between the sample and zone plate. The OSA is used to block out unwanted diffraction orders from the zone plate. The sample is mounted on top of a high-resolution piezostage. During regular STXM image acquisition, the piezoscanner is used to raster-scan the specimen through the focus produced by the zone plate. A laser doppler displacement measuring system (LDDM) measures the relative position of the focusing optics and the sample module in the x- and y-directions with <1 nm resolution. The detector module consists of a motorized XYZ stage stack. A mounting platform on top provides space for three detectors (x-ray detector, photodiode, and visible light microscope), which can be inserted in or moved out from the beam with the control software. The x-ray detector is a scintillator-photomultiplier tube. The scintillator converts the x rays into visible light, which is then detected with the photomultiplier tube (PMT). The counts from the PMT are then amplified and processed by the motion controller as the detector input during the scans.

III. COMMISSIONING RESULTS

A. Photon flux at sample

The photon flux at the sample (focusing position) was characterized by an AXUV100G photodiode. The lower energy photons ranging from 250 to 750 eV used the first harmonic, while the higher energy photons from 750 to 2000 eV used the third harmonic radiation from the EPU. Figure 3 shows the measured photon flux normalized to a beam cur-

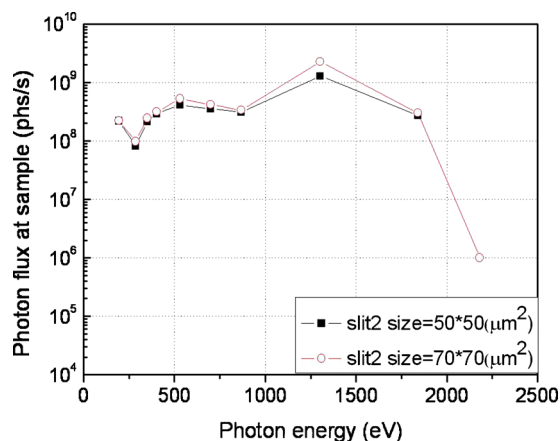


FIG. 3. (Color online) The photon flux at the sample normalized to a beam current of 200 mA with an exit slit of $50 \times 50 \mu\text{m}^2$ (solid) and $70 \times 70 \mu\text{m}^2$ (open).

rent of 200 mA. A photon flux larger than 10^8 photons/s was achieved over the entire range, except at the carbon K-edge due to carbon contamination of the optical components. The transmission efficiency of the STXM was estimated to be 0.6% at 400 eV and 3% at 1800 eV including the loss of the Si_3N_4 window, the absorption, and the diffraction efficiency of the zone plate with its outmost zone width of 30 nm.

B. Energy resolving power

An ion chamber was designed and fabricated to evaluate quantitatively the energy resolving power for the beamline by measuring the shell excitation spectrum of various gases (Ar, N_2).^{15–17} The gas pressure in the ion chamber was 2×10^{-3} Torr and the voltage between the anode and cathode was 28 V. The photocurrent was measured with a Keithley 6485 picoammeter. Figure 4(a) shows the Ar $L_{2,3}$ absorption edge. The Ar $L_{2,3}$ absorption edge $2p_{3/2}^{-1} \rightarrow nl$ and $2p_{1/2}^{-1} \rightarrow nl$ Rydberg states and the fine structures $2p_{3/2} \rightarrow 4s, 3d, 4d, 5d, 6d, 7d$ and $2p_{1/2} \rightarrow 4s, 3d, 4d, 5d, 6d, 7d$ were observed. In addition, the 7d peaks were clearly present in the spectra. The observed spectral line is a convolution between Lorentzian and Gaussian profiles (Voigt profile). The Gaussian broadening for the profile is usually attributed to the beam-

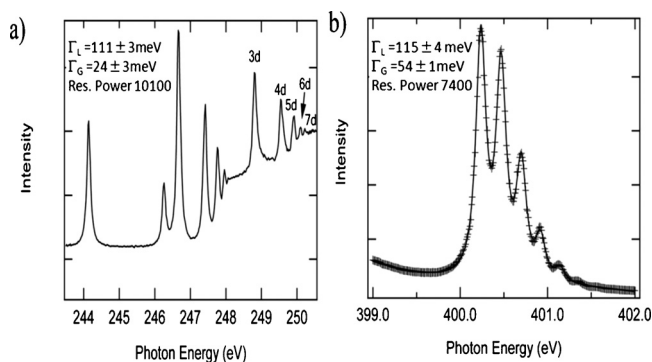


FIG. 4. The excitation spectra of Ar and N_2 gas measured using the first grating (800 lines/mm groove density) with $c_{\text{eff}} = 1/2.5$.

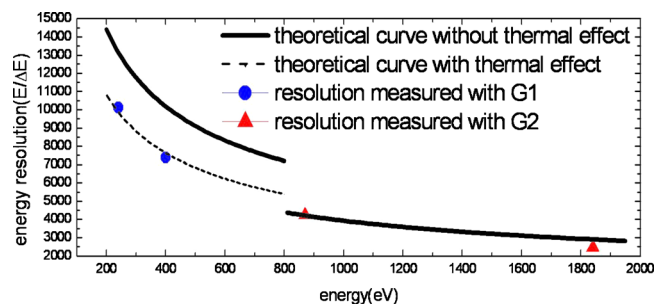


FIG. 5. (Color online) Theoretical curve and experimental data of energy resolution.

line instruments, whereas the Lorentzian is generally taken as the natural linewidth. The energy resolving power of the beamline was estimated by

$$E/\Delta E = E/\Gamma_G, \quad (1)$$

where the Gaussian broadening is denoted as Γ .

The $2p_{3/2}^{-1} \rightarrow 4s$ peak of argon was fit using the Voigt profile,

$$y = y_0 + A \frac{2 \ln 2 \Gamma_L}{\pi^{3/2} \Gamma_G^2} \times \int_{-\infty}^{\infty} \frac{e^{-t^2}}{\left(\sqrt{\ln 2} \frac{\Gamma_L}{\Gamma_G} \right)^2 + \left(\sqrt{4 \ln 2} \frac{x - x_c}{\Gamma_G} - t \right)^2} dt, \quad (2)$$

where the Lorentz width Γ_L is 111 ± 3 meV (Ref. 18) and the Gaussian width Γ_G is 24 ± 3 meV. Therefore, the resolving power can be readily calculated to be 10 100.

The shell excitation spectrum of N_2 is shown in Fig. 4(b). The N_2 ($\text{N } 1s, v=0$) $\rightarrow (\pi_g^*, v'=1)$ transition energy of 401.10 eV reported by Sodhi and Brion¹⁹ was used as the reference for the incident photon energy. As shown in Fig. 4(b), the structures attributed to N_2 ($\text{N } 1s, v=0$) $\rightarrow (\pi_g^*, v': v'=0-5)$ transitions were clearly resolved. The Lorentz and Gaussian widths were set to be equal for the six peaks. By fitting the experimental curve with Voigt functions, we obtained a Lorentzian width of $\Gamma_L = 115 \pm 4$ meV (Ref. 20) and a Gaussian width of $\Gamma_G = 54 \pm 1$ meV.

It is difficult to get an exact energy resolving power at higher photon energy because no suitable gas can be used. Nevertheless, the Si K-edge spectrum of Si_3N_4 was used to be as a rough guide of this value. This was done by fitting the differential curve of the 100 nm thick Si_3N_4 transmission spectra with Voigt function. The Lorentz width and the

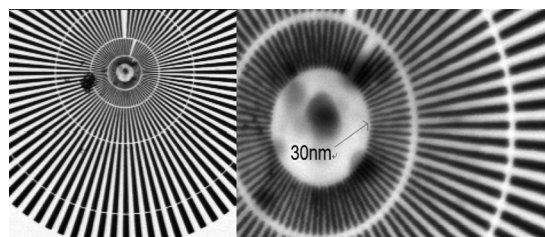


FIG. 6. Image of the test pattern sample scanned by STXM with a scanning range of $5 \mu\text{m} \times 3 \mu\text{m}$ and a scanning step of 15 nm. The inner circle demonstrates a spatial pattern of 30 nm.

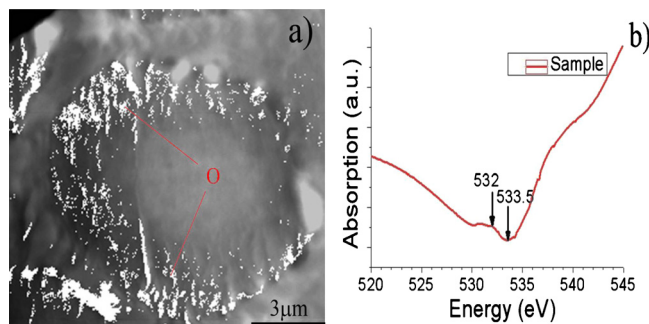


FIG. 7. (Color online) The spatial distribution of oxygen in the preoxidized PAN fiber cross-section using STXM.

Gaussian width are 1.4 eV and 747 meV, respectively, and the resolving power could be rather roughly estimated to be above 2400 at 1840 eV (Si K-edge).

The solid lines in Fig. 5 show the theoretical calculation without consideration of the thermal deformation due to the high heat load. It is easily found that the thermal deformation degrades the energy resolution severely at lower photon energy range. If this influence was considered to be equivalent to a heat-load-induced slope error for the premirror in the monochromator, then this induced slope error can be estimated to be 1.2 μ rad by fitting the experimental data, as the dotted line shows. This value is consistent with the ANSYS analysis.

C. Spatial resolution

The focusing element (the zone plate) was made by Xradia. It has a radius of 200 μ m, an outmost zone width of 30 nm, and a central stop diameter of 20 μ m. The electroplated zone material is gold and is located on a 100 nm Si_3N_4 substrate. The transmission efficiency of the focusing system, including the zone plate and the OSA, was measured to be about 2% at an energy of 401 eV. A test sample provided by Xradia was scanned with an energy of 870 eV and a beam

current of 170 mA. With a fine scanning step of 15 nm, the fine image of the center area of the sample was measured (Fig. 6). The inner circle can be clearly seen, including the finest strips that have a width of 30 nm, demonstrating that the spatial resolution is better than 30 nm. In this measurement, the exit slit size was set to be 20 $\mu\text{m} \times 20 \mu\text{m}$.

IV. PRELIMINARY EXPERIMENT

After a few months from its commissioning, the beam-line was already in operation and some experiments had been performed. With its excellent ability for chemical analysis and submicron spatial resolution, we have obtained some preliminary experimental results.

A. Two-dimensional scan and point spectrum

Figure 7 shows the spatial distribution of oxygen elements in the preoxidized PAN fiber cross-section.²¹ The typical STXM transmission image of sample was scanned in two dimensions over the range of 13 $\mu\text{m} \times 13 \mu\text{m}$, with a step of 50 nm and a dwell time of 10 ms at 532 and 533.5 eV. The energies were selected as being before and after the absorption edge of oxygen, respectively, and were based on the K-edge NEXAFS spectra of oxygen [Fig. 7(b)], which were measured with a one-dimensional point spectrum scan over an energy range of 520–545 eV and with a step 0.15 eV. The final result [Fig. 7(a)] was obtained by subtracting the energy with a contrast imaging technique, thereby highlighting the oxygen distribution due to the absorption difference in the preoxidized PAN fiber cross-section.

B. Scan stack

Figure 8 shows results from a study of automobile exhaust particles by STXM.²² A single particle was chosen as a typical example as shown in the top right corner. Using stack scan in the range of 2 $\mu\text{m} \times 2 \mu\text{m}$ with step of 50 nm and dwell time of 2 ms, we scanned the energy from 396 to 416

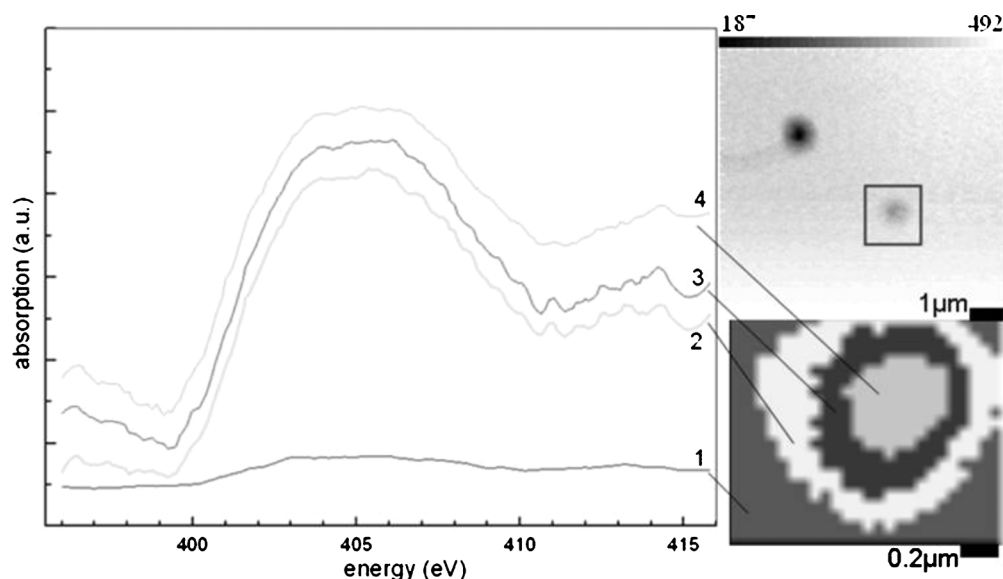


FIG. 8. Results from stack scan experiments on an automobile exhaust particle, which was determined to have four components by PCA and CA. The NEXAFS spectra and distributions of the four components are shown.

eV with a step of 0.12 eV to produce a series of energy stack images. Conventional principal component analysis (PCA) and cluster analysis (CA) revealed that there were four clusters in the sample: the background, the surface of automobile exhaust particle, the middle layer of the particle, and the center of the particle. There are some differences between the inside and outside of the automobile exhaust particle. The surface of the particle shows sharper peaks at 401.7 eV and 405.7 eV corresponding to the components of nitrates; by contrast, the inside of the particle shows wider σ^* resonances at 406 eV corresponding to the ammonium and also absorbs at 396.5 eV due to the organic nitrogen compounds. The NEXAFS spectrum of the middle layer was similar to that of the inside layer over the energy range 407–415 eV and similar to the surface layer over the energy range 396–407 eV. The middle layer is a transitional region between the inner and outer layers and mainly consists of nitrates and organic nitrogen compounds.

V. SUMMARY

A high performance soft x-ray beamline was successfully constructed at SSRF, which allows experiment carried out with both high spatial and high energy resolutions. By using a variable-included-angle plane grating monochromator with two gratings, the photon energy can cover from 200 to 2000 eV. The energy resolving power was also quantitatively estimated, showing this value can be better than 10 000 at low photon energy. The spatial resolution was measured to be better than 30 nm. Unfortunately the circular polarization for EPU has not been characterized due to the time restriction for commissioning, which is anticipated to be conducted soon.

ACKNOWLEDGMENTS

The authors are grateful to Dr. Tony Warwick (ALS), Dr. Tolek Tyliczszak (ALS), Dr. Mochizuki Tetsuro (JASRI), Dr. Konstantine Kaznatcheev (CLS), Dr. Wenbing Yun (Xradia), Professor Ito Kenji (PF), Professor Ando Masami (PF), Professor Miyahara Tsuneaki (Tokyo Metr. U.), and Professor Adam Hitchcock (CLS) for their kind help and suggestions of this beamline and end-station during design and construction.

- ¹L. D. Kilcoyne, T. Tyliczszak, W. F. Steele, S. Fakra, P. Hitchcock, K. Franck, E. Anderson, B. Harteneck, E. G. Rightor, G. E. Mitchell, A. P. Hitchcock, L. Yang, T. Warwick, and H. Ade, *J. Synchrotron Radiat.* **10**, 125 (2003).
- ²U. Wieseemann, J. Thieme, P. Guttman, B. Niemann, D. Rudolph, and G. Schmahl, *AIP Conf. Proc.* **507**, 430 (2000).
- ³T. Beetz, M. Feser, H. Fleckenstein, B. Hornberger, C. Jacobsen, J. Kirz, M. Lerotic, E. Lima, M. Lu, D. Sayre, D. Shapiro, A. Stein, D. Tennant, and S. Wirick, *Synchrotron Radiat. News* **16**, 11 (2003).
- ⁴B. Kaulich, D. Bacescu, D. Cocco, J. Susini, M. Salomé, O. Dhez, C. David, T. Weitkamp, E. D. Fabrizio, S. Cabrini, G. Morrison, P. Charalambous, J. Thieme, T. Wilhein, J. Kovac, M. Podnar, and M. Kiskinova, *J. Phys. IV* **104**, 103 (2003).
- ⁵K. V. Kaznatcheev, Ch. Karunakaran, U. D. Lanke, S. G. Urquhart, M. Obst, and A. P. Hitchcock, *Nucl. Instrum. Methods Phys. Res. A* **582**, 96 (2007).
- ⁶H.-J. Shin and M. K. Lee, *Nucl. Instrum. Methods Phys. Res. A* **467–468**, 909 (2001).
- ⁷J. M. Kenney, G. R. Morrison, M. T. Browne, C. J. Buckley, R. E. Burge, R. C. Cave, P. S. Charalambous, P. J. Duke, A. R. Hare, C. P. B. Hills, A. G. Michette, K. Ogawa, and A. M. Rogoyski, *J. Phys. E* **22**, 234 (1989).
- ⁸B. Van Waeyenberge, A. Puzic, H. Stoll, K. W. Chou, T. Tyliczszak, R. Hertel, M. Föhnle, H. Bruckl, K. Rott, G. Reiss, I. Neudecker, D. Weiss, C. H. Back, and G. Schütz, *Nature (London)* **444**, 461 (2006).
- ⁹Y. Acremann, J. P. Strachan, V. Chembroli, S. D. Andrews, T. Tyliczszak, J. A. Katine, M. J. Carey, B. M. Clemens, H. C. Siegmann, and J. Stöhr, *Phys. Rev. Lett.* **96**, 217202 (2006).
- ¹⁰A. Braun, *J. Environ. Monit.* **7**, 1059 (2005).
- ¹¹S. Bernard, K. Benzerara, O. Beyssac, N. Menguy, F. Guyot, G. E. Brown, Jr., and B. Goffé, *Earth Planet. Sci. Lett.* **262**, 257 (2007).
- ¹²H. Petersen, *Opt. Commun.* **40**, 402 (1982).
- ¹³F. Riemer and R. Torge, *Nucl. Instrum. Methods* **208**, 315 (1983).
- ¹⁴A. V. Pimpale, S. K. Deshpande, and V. G. Bhide, *Appl. Opt.* **30**, 1591 (1991).
- ¹⁵G. C. King, M. Tronc, F. H. Read, and R. C. Bradford, *J. Phys. B* **10**, 2479 (1977).
- ¹⁶M. Kato, Y. Morishita, M. Oura, H. Yamaoka, Y. Tamenori, K. Okada, T. Matsudo, T. Gejo, I. H. Suzuki, and N. Saito, *J. Electron Spectrosc. Relat. Phenom.* **160**, 39 (2007).
- ¹⁷A. P. Hitchcock and C. E. Brion, *J. Electron Spectrosc. Relat. Phenom.* **18**, 1 (1980).
- ¹⁸K. C. Prince, M. Vondráček, J. Karvonen, M. Coreno, R. Camilloni, L. Avaldi, and M. de Simone, *J. Electron Spectrosc. Relat. Phenom.* **101–103**, 119 (1999).
- ¹⁹R. N. S. Sodhi and C. E. Brion, *J. Electron Spectrosc. Relat. Phenom.* **34**, 363 (1984).
- ²⁰M. Vondráček, K. C. Prince, J. Karvonen, M. Coreno, R. Camilloni, L. Avaldi, and M. de Simone, *Synchrotron Radiat. News* **12**, 4 (1999).
- ²¹X. Z. Zhang, Z. J. Xu, R. Z. Tai, X. J. Zhen, Y. Wang, Z. Guo, R. Yan, R. Chang, B. Wang, M. Li, J. Zhao, and F. Gao, “Ratio-contrast imaging of dual-energy absorption for element mapping with a scanning transmission x-ray microscope,” *J. Synchrotron Radiat.* (in press).
- ²²C. J. Yang, Z. Guo, X. Z. Zhang, R. Z. Tai, L. M. Bao, X. L. Li, G. L. Zhang, and Y. Li, “The study of automobile exhaust particles by spectro-microscopy,” *Nucl. Sci. Technol.* (in press).